Micrometer-sized Monodispersed Silica Spheres with Advanced Adsorption Properties

Y. Chen, Y. J. Wang, L. M. Yang, and G. S. Luo
The State Key Laboratory of Chemical Engineering, Dept. of Chemical Engineering, Tsinghua University, Beijing, 100084, China

DOI 10.1002/aic.11359
Published online December 3, 2007 in Wiley InterScience (www.interscience.wiley.com).

Micrometer-sized monodispersed mesoporous silica spheres with adjustable particle diameter and adjustable pore structure were successfully prepared. Drops of a silica sol were injected by a microfluidic device into a heated oil bath where the droplets solidified during sedimentation. Drop size was varied by control of the rates of the oil flow past the silica sol injector. The silica sol was made by prehydrolysis of tetraethyl orthosilicate (TEOS) in an aqueous acidic solution using a triblock copolymer as the template. Acrylamide monomer was added in the sol after prehydrolysis to accelerate the solidification rate of drops in the oil bath. The amount of monomer was used to control the pore sizes in the silica particles. The effect of synthesis conditions on the morphology and pore structure of spheres was investigated. Silica spheres with different surface morphology and internal structure were obtained by changing the composition of sedimentation medium. Pore diameter and pore-size distribution can be adjusted effectively by controlling the concentration of silica source, acid or polymeric monomer in the aqueous phase. The prepared silica spheres have high-surface area (>550 m^2/g), large pore volume (>1.1 cm^3/g) and large amount of macropores. High-protein adsorption capacity (520mg/g) was achieved in the adsorption experiments of bovine serum albumin (BSA). Pore structure of silica spheres was demonstrated to be a crucial factor to determine the protein adsorption capacity. © 2007 American Institute of Chemical Engineers *AIChE J,* 54: 298–309, 2008

Keywords: mesoporous, silica sphere, microfluidic device, sedimentation polymerization, protein adsorption

Introduction

Since the synthesis of M41S materials in 1992,[1,2] the mesoporous silica with controlled nanostructure and macroscopic morphologies have attracted much attention because of their emerging applications in the areas of catalysis, adsorption, chromatography, and controlled release of drugs.[3,4] Among the particles with all kinds of morphologies, micrometer-sized monodisperse silica spheres are very promising.

Mesoporous inorganic materials are viewed as ideal candidates as hosts of biomolecules, because they fulfill many of the requirements for enzyme carriers, such as high-surface area, large pore volume, hydrophilic character, chemical and thermal stability, mechanical strength, suitable particle form, regenerability and toxicological safety.[5] Mesoporous silica materials were once used to capture small proteins (ca. <45 kDa),[6] such as cytochrome c,[7–11] lysozyme,[12–14] and trypsin[15,16] for their relatively small pore size. With the emergence of mesoporous materials with large pores, such as

Correspondence concerning this article should be addressed to G. S. Luo at gsluo@tsinghua.edu.cn.

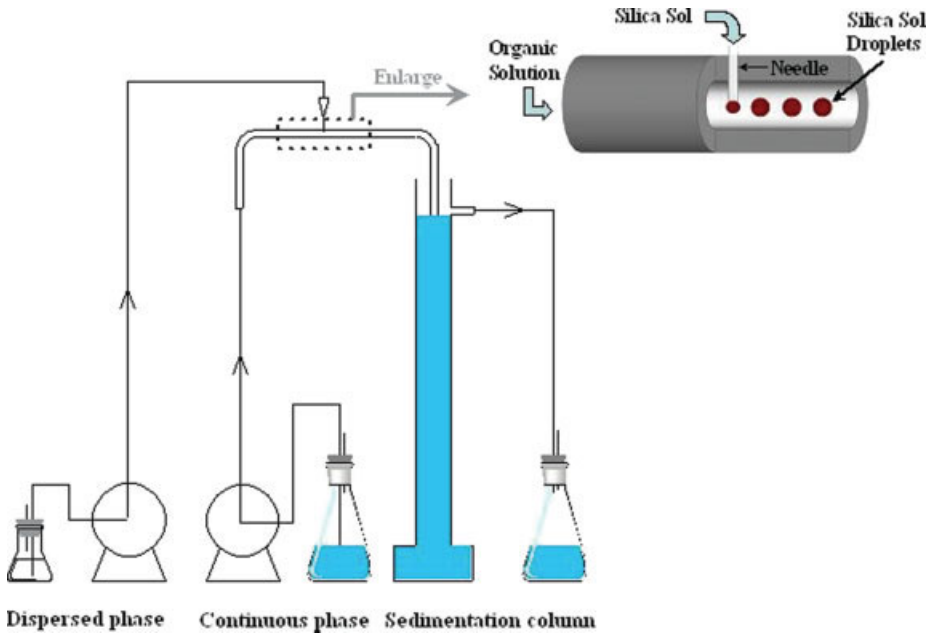

Figure 1. Experimental device.

[Color figure can be viewed in the online issue, which is available at www.interscience.wiley.com.]

SBA-15/16, materials using swelling agents or mesocellular foams (MCF), adsorption capacity of large proteins, such as bovine serum albumin (BSA),[17] penicillin G acylase,[18] chloroperoxidase (CPO)[19] and α-amylase[20] has significantly increased. Mesoporous silica materials with larger pores are investigated to achieve the inclusion of large biomolecules, or the improvement of protein loading. However, most research work focused on the adsorption of small size spheres, which is not easily applied in large-scale separation processes of biomolecules.

The synthesis of monodisperse micrometer-sized mesoporous silica spheres with relatively large size is still a challenge work.[21–41] Recently, microfluidic devices have been reported to produce monodispersed droplets, and, subsequently, to create polymeric microparticles[42–50] and hollow capsules[44,51] by photopolymerization or interfacial polymerization. Synthesis in microfluidic devices provides a powerful strategy for continuous, reproducible, and scalable production of inorganic, organic, and bioorganic products. However, unlike polymer synthesis,[42–51] traditional synthesis of mesoporous silica involves a sol-gel process, which is time-consuming, and, consequently, not easily controlled in microfluidic devices. Here, we describe the microfluidic-based synthesis of monodisperse mesoporous silica spheres with uniform and optionally adjustable diameter larger than 100 μm. In the new process a working system based on sedimentation polymerization was developed,[33,34,52] and a microfluidic device[49] was applied to control the dispersed droplet size. The main purpose is to prepare silica spheres with large diameter and adjustable pore structure for large-scale separation of biomolecules. The effect of synthesis conditions, such as the composition of silica sol, aqueous phase and sedimentation medium on the surface morphology, internal structure and pore size of silica spheres has been investigated. High-protein adsorption capacity has been obtained by the micrometer-sized silica spheres. The influence of pore size on loading capacity of BSA has been determined.

Experimental

Materials

Bovine serum albumin (BSA), acrylamide, *N,N′*-methylene bisacrylamide and ammonium persulfate were purchased from Biodee Biotechnology Co., Ltd. (Beijing, China). Triblock copolymer F127 ($EO_{106}PO_{70}EO_{106}$) was produced by Sigma-Aldrich Corporation (USA). Tetraethyl orthosilicate (TEOS) was produced by Xilong Chemical Co., Ltd. (Shantou, China). Liquid paraffin was obtained from Bodi Chemicals Co., Ltd. (Tianjin, China). Sorbitan trioleate (Span 85) was obtained from China Medicine (Group)

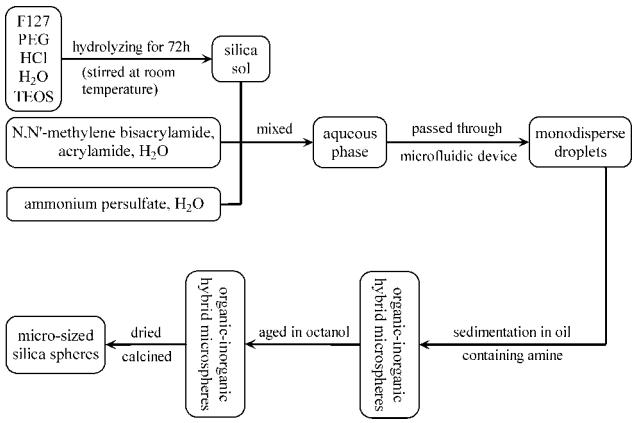

Figure 2. Synthesis route.

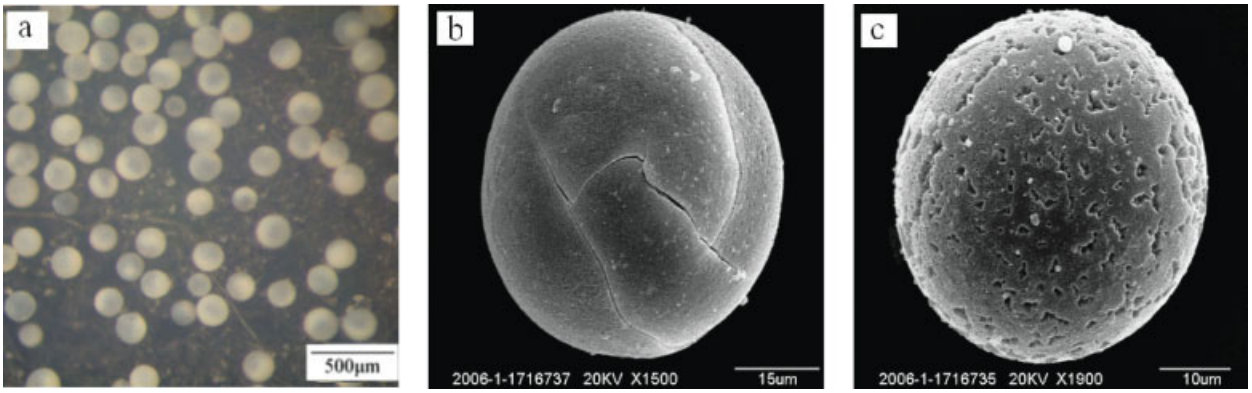

Figure 3. Optical image (a), and SEM images (b, c) of silica spheres synthesized with direct gelation.

[Color figure can be viewed in the online issue, which is available at www.interscience.wiley.com.]

Shanghai Chemical Reagent Corporation (Shanghai, China). Tri-octylamine (TOA) was produced by Feixiang Chemicals Co., Ltd. (Zhangjiagang, China). Hydrochloric acid (HCl, 36.5 wt %) and acetone were produced by Beijing Chemical Company (Beijing, China). Poly(ethylene glycol) (PEG 20000) was obtained from Yili Fine Chemical Co., Ltd. (Beijing, China). Octanol, Acetic acid (HAc) were obtained from Xiandai Dongfang Chemicals Co., Ltd. (Beijing, China). All materials were chemically pure.

Synthesis of silica spheres

The scheme of the experimental device is shown in Figure 1. The continuous oil phase flowed in Teflon tubing (1.5 mm ID $\times$ 2.0 mm OD); the dispersed aqueous phase was introduced via a needle (0.2 mm ID $\times$ 0.7 mm OD) inserted halfway into the tubing. The glass sedimentation column was 75 cm in length, having an internal diameter of 2 cm.

The scheme of the synthesis route is shown in Figure 2. The silica sol was typically prepared as following: 1.5 g of triblock copolymer F127 ($EO_{106}PO_{70}EO_{106}$, SIGMA), and 3.0 g of PEG20,000 (poly(ethylene glycol)) were dissolved under stirring in 5.0 g 0.1 M HCl aqueous solution, then 15 g of tetraethyl orthosilicate (TEOS) was added. The resultant mixture was stirred for three days at room-temperature to obtain a clear silica sol. Silica sol with various TEOS/H_2O ratios was obtained by shifting the amount of water and TEOS. The aqueous polymeric monomer solution was prepared from acrylamide (15.0 g), *N,N′*-methylene bisacrylamide (3.0 g, crosslinker, based on acrylamide) and deionized water (20.0 g). The ammonium persulfate was used as the initiator whose aqueous solution (20 wt %) was prepared from ammonium persulfate and deionized water. The dispersed aqueous phase was the mixture of the silica sol, the polymeric monomer solution and the initiator solution. Typically, 2.0 g aqueous polymeric monomer solution, and 0.2 g ammonium persulfate aqueous solution were added to 5.0 g silica sol. The mixture was stirred for five minutes, and then centrifugated to remove the bubbles. The continuous oil phase was liquid paraffin containing 2 wt % span85. The sedimentation medium was a liquid paraffin solution containing 2 wt % span85 and 30 wt % trioctylamine (TOA). TOA acted as an alkali and extracted HCl from aqueous phase.

The aqueous mixture (dispersed phase) was dispersed into continuous oil phase to form monodispersed droplets by a microfluidic device at certain flow rates (typically the flow rate of dispersed phase was 0.02 mL/min, the flow rate of continuous phase was 0.2 mL/min). Then the droplets flowed into the sedimentation medium (75 °C), and were rapidly solidified (1–2 min). After sedimentation, the organic-inorganic hybrid spheres were kept in the sedimentation column for 30 min. Then they were filtered and transferred into an autoclave. 10 mL of octanol and 5mmol acetic acid were added into the autoclave at the same time. Here acetic acid was used to neutralize the residual amine and keep the acidic environment. The spheres were, subsequently, treated at 100°C for 24 h to complete the polymerization of acrylamide and the gelation of silica. Finally, the solid product was washed with acetone, air-dried at 80 °C overnight, and then calcined at 550 °C for 6 h to remove the template and polymer.

Characterization of silica spheres

Scanning electron microscopy (SEM) observations were performed on a JEOL JSM 7401F microscope operating at 1.0 kV. Nitrogen adsorption-desorption isotherms were measured at 77 K using a Quantachrome Autosorb-1-C Chemisorption-Physisorption Analyzer. Before measurement, the silica spheres were outgassed at 200 °C for 40 min, and the protein loaded samples were outgassed at 35 °C for 24 h. The BET surface area was calculated from the adsorption branches in the relative pressure range of 0.05–0.25, and the total pore volume was evaluated at a relative pressure of about 0.995. The pore-size distributions were calculated from the adsorption branches using the Barrett-Joyner-Halenda (BJH) method. Intrusion volumes and pore-size distributions were recorded by the mercury intrusion method using a Micromeritics Autopore IV 9510 porosimeter.

Protein adsorption

Adsorption experiments were carried out by contacting 50 mg of silica spheres with 10 mL of solution containing 10 mg/mL BSA in pH 5.0, 50 mM acetate buffer. The

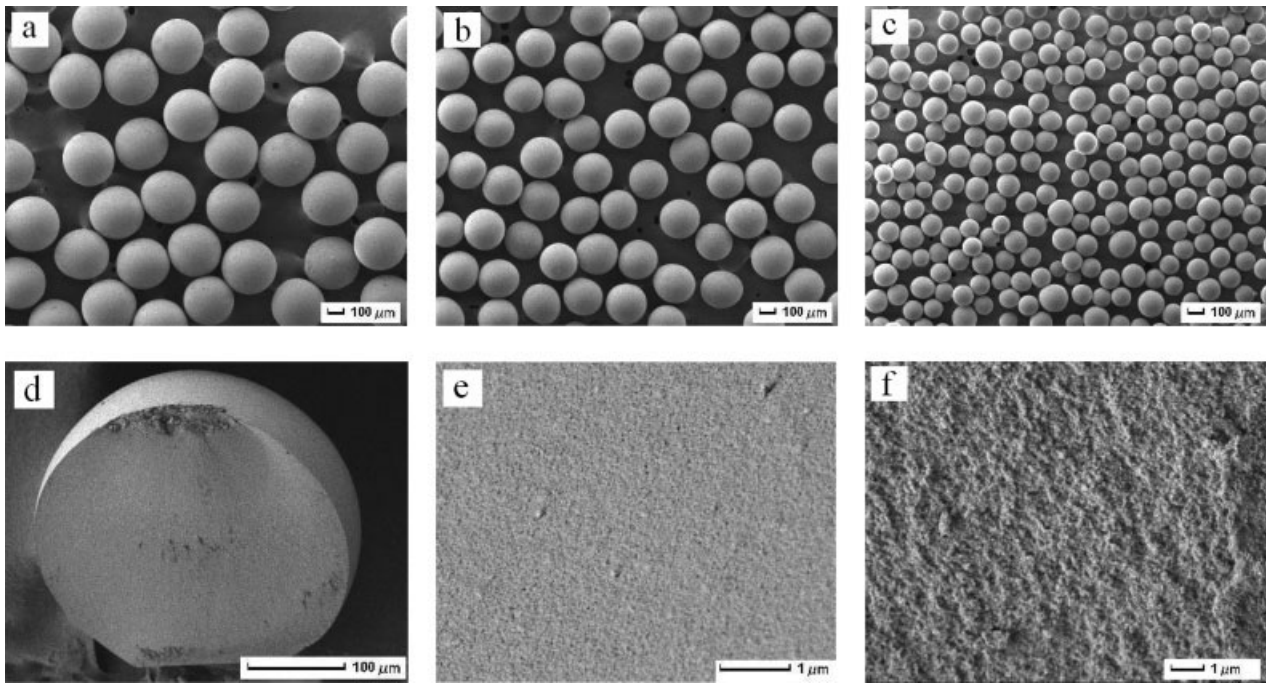

Figure 4. SEM images of silica spheres based on sedimentation polymerization: (a–c) synthesized with a flow rate of 0.02 mL/min for dispersed phase, and various flow rates for continuous phase: (a) 0.2 mL/min; (b) 0.4 mL/min; (c) 1.6 mL/min; (d–f) synthesized with a flow rate of 0.02 mL/min for dispersed phase and 0.2 mL for continuous phase: (d) a single cross-sectioned silica sphere; (e) silica sphere surface; (f) internal structure of silica sphere.

(In the silica sol, TEOS/H_2O (w/w) = 30, HCl/H_2O = 100 mmol/L; in the aqueous phase, silica sol/monomer solution (w/w) = 2.5; the sedimentation medium contains 30 wt % TOA.)

adsorbent and solution were shaken in a HZS-H Environmental Incubator Shaker (Harbin Donglian Electronic & Technology Development Co., Ltd. of China) at 160 rpm and 25°C until equilibrium was reached (typically 96 h). The protein concentration in the solution was analyzed using a UV Spectrophotometer (HP 8453, Agilent) at 280 nm, and a mass balance was applied to calculate the amount of BSA adsorbed on the silica spheres. In this experiment, several kinds of silica spheres with different pore structures were tested to investigate the effect of pore size on the protein adsorption.

Results and Discussion

Synthesis of silica spheres

In our previous research,[33,34] a new "pH-induced rapid colloid aggregation" method was developed to synthesize micrometer-sized mesoporous silica spheres, in which pluronic triblock copolymer and poly(ethylene glycol) (PEG), or their mixtures were used as templates, and a stable silica sol was obtained during the prehydrolysis process. However, in this work the silica sol can hardly gelate before the droplets reach the bottom of sedimentation column by the "pH-induced rapid colloid aggregation" method. Therefore, silica spheres synthesized by direct gelation of silica sol showed weak mechanical stability, some of which were even cracked (as shown in Figure 3).

To control the fabrication of silica spheres more efficiently, polymerization reaction of acrylamide (AM) was introduced to the silica sol system. The mixture of silica sol, aqueous polymeric monomers and initiator solution was dispersed to monodisperse droplets using the aforementioned

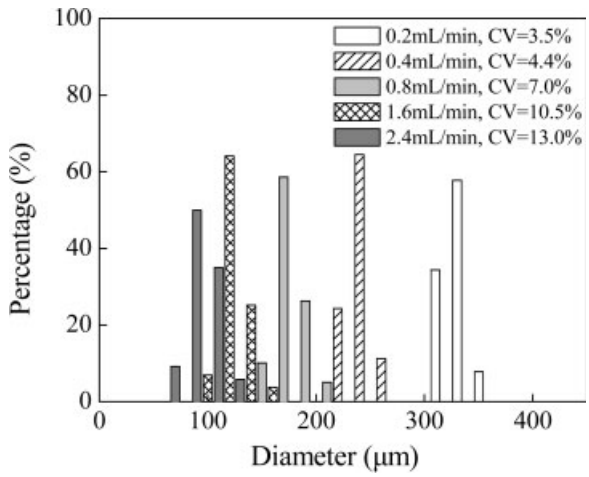

Figure 5. The particle-size distributions of various samples synthesized with a flow rate of 0.02 mL/min for dispersed phase and various flow rates for continuous phase.

(In the silica sol, TEOS/H_2O (w/w) = 3.0, HCl/H_2O = 100 mmol/L; in the aqueous phase, silica sol/monomer solution (w/w) = 2.5; the sedimentation medium contains 30 wt % TOA.)

microfluidic device, and injected into a glass column containing a hot oil sedimentation medium. Trioctylamine (TOA) was used to extract HCl from droplets and accelerate the polymerization reaction. During the sedimentation process, the aqueous polymeric monomers polymerized rapidly to form monodispersed spheres in the hot oil sedimentation medium. The silica sol was retained in spheres and gelated gradually.

The SEM images of resultant mesoporous silica spheres synthesized under typical synthesis conditions after calcination are shown in Figure 4. Through adjusting the size of silica sol droplets, which can be controlled by the flow rate of continuous and dispersed phases, monodisperse silica spheres with different scale of diameters in the range from several tens to several hundreds of micrometers have been obtained (shown in Figure 4a–c). In Figure 5, the particle-size distributions of various samples are plotted, and the coefficients of variations (CV, the standard deviations of the diameter) of the diameters are given. The mean particle sizes decrease, and CV of the diameter increases as the flow rate of the continuous phase increases. Figure 4d shows a single cross-sectioned silica sphere, which reveals that the silica spheres are solid. Figure 4e and 4f show the external surface and the internal structure of the silica spheres separately, from which the compact and dense structure of silica spheres can be seen distinctly.

Surface morphology and internal structure

Monodispersed silica spheres with different surface morphology and internal structure have been synthesized under various synthesis conditions. The concentration of polymeric monomer in the aqueous phase is the key factor of the synthesis. With the increase of the polymeric monomer concentration, the solidification of droplets goes faster. Droplets solidified in one minute to form the organic-inorganic hybrid spheres when the concentration of monomer reached 9 wt % in the aqueous phase (silica sol/monomer solution = 4). After calcination, the monodisperse porous silica spheres were obtained.

The SEM images of silica spheres synthesized with different polymeric monomer concentration in the aqueous phase are shown in Figure 6. The solid, compact and dense struc-

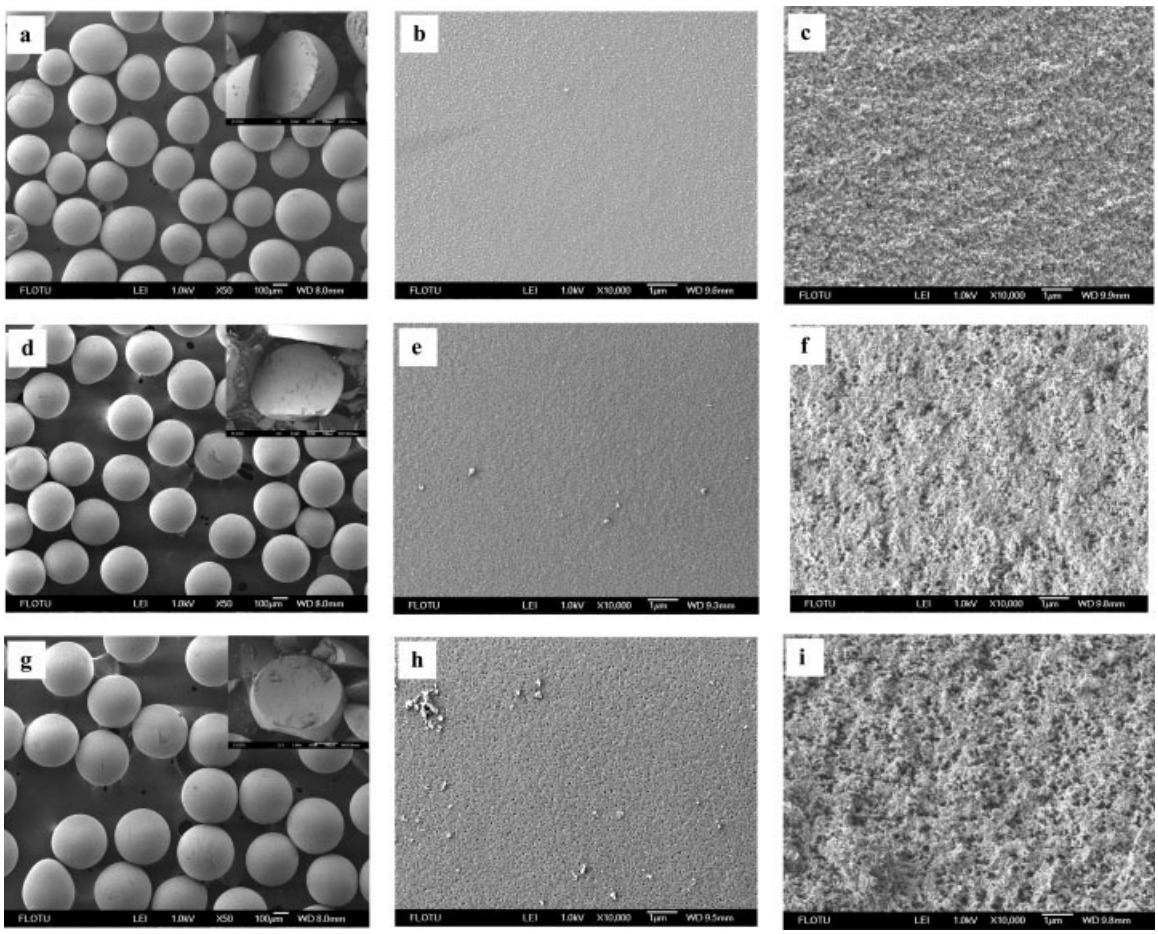

Figure 6. SEM images of spheres with different silica sol/monomer solution (w/w) in the aqueous phase: (a–c) silica sol/monomer solution = 4.0, (d-f) silica sol/monomer solution = 2.5, (g–i) silica sol/monomer solution = 1.7; (a, d, g), the inset is the cross-section of a single silica sphere, (b, e, h) silica sphere surface, (c, f, i) internal structure of silica sphere.

(In the silica sol, TEOS/H_2O(w/w) = 3.0, HCl/H_2O = 100 mmol/L; the sedimentation medium contains 30 wt % TOA.)

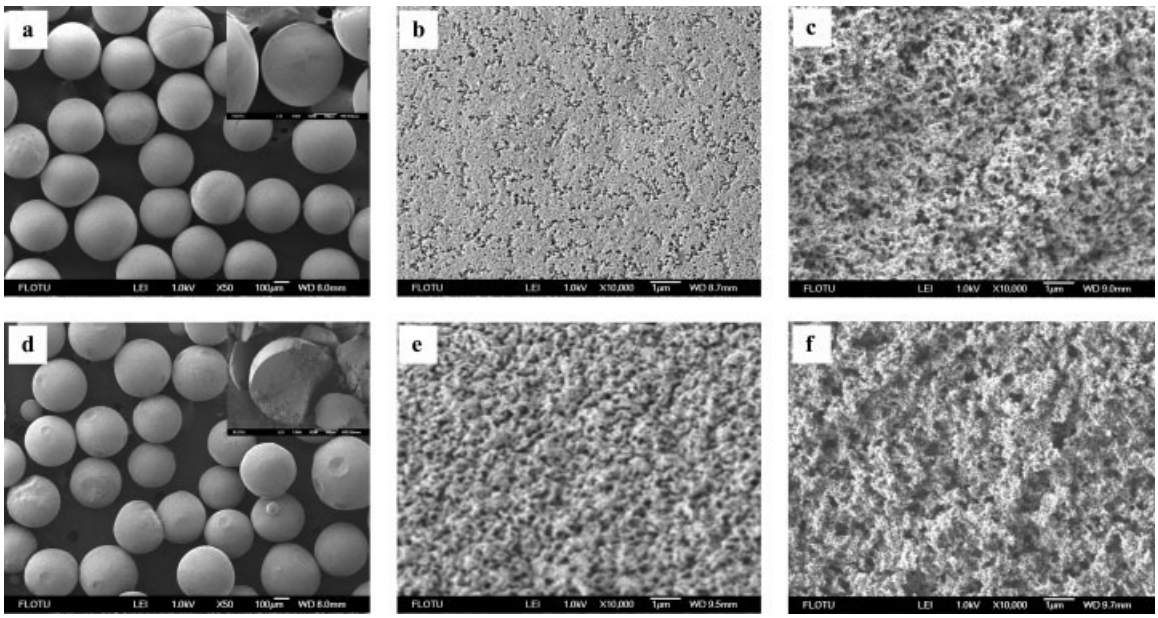

Figure 7. SEM images of spheres with different TEOS/H_2O (w/w) in the silica sol: (a–c) TEOS/H_2O = 1.5, (d–f) TEOS/H_2O = 0.5; (a, d) the inset is the cross-section of a single silica sphere, (b, e) silica sphere surface, (c, f) internal structure of silica sphere.

(In the silica sol, HCl/H_2O = 100 mmol/L; in the aqueous phase, silica sol/monomer solution (w/w) = 2.5; the sedimentation medium contains 30 wt % TOA.)

ture of silica spheres can be seen from the cross-section, external surface and internal structure. With the increase of the monomer concentration in the aqueous phase, organic polymers occupy more space in the hybrid spheres, the structure of silica spheres after removal of polymer becomes a little looser, and some texture pores (microscopic pores in the external skin and cross-section of silica spheres) appear.

The composition of silica sol is another important factor influencing the surface morphology and internal structure of silica spheres. The SEM images of samples synthesized

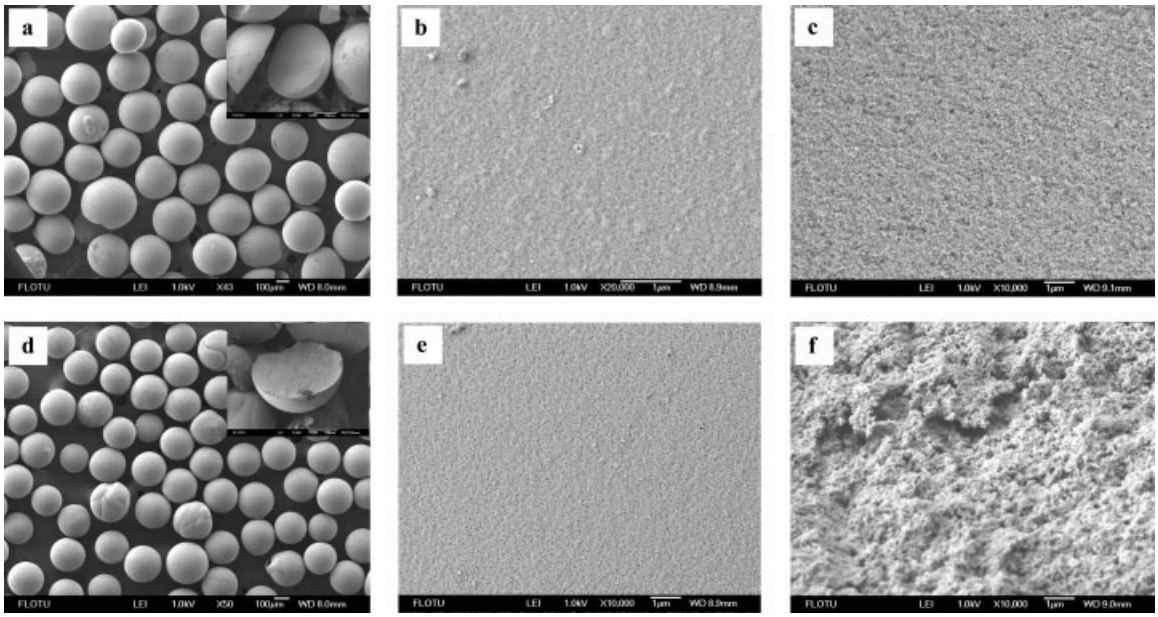

Figure 8. SEM images of spheres with lower HCl concentration in the silica sol: (a–c) TEOS/H_2O = 3.0, (d–f) TEOS/H_2O = 1.5; (a, d) the inset is the cross-section of a single silica sphere, (b, e) silica sphere surface, (c, f) internal structure of silica sphere.

(In the silica sol, HCl/H_2O = 10 mmol/L; in the aqueous phase, silica sol/monomer solution (w/w) = 2.5; the sedimentation medium contains 30 wt % TOA.)

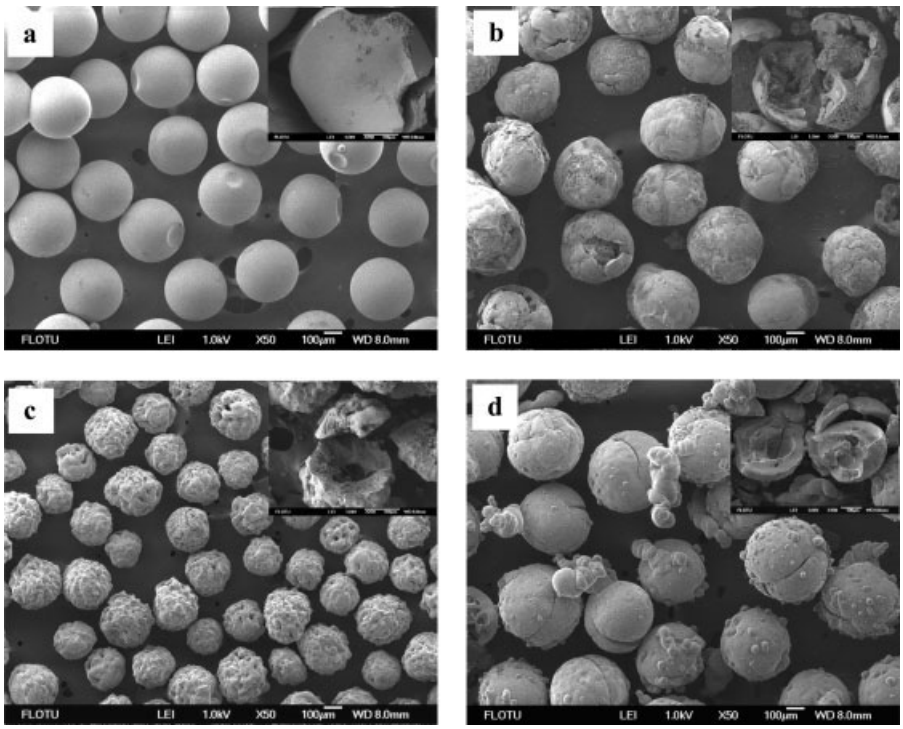

Figure 9. SEM images of spheres with different compositions in the sedimentation medium: (a) 5 wt % TOA, (b) 5 wt % TOA + 10 wt % octanol, (c, d) 30 wt % TOA + 30 wt % TBP; (a–d) the inset is the cross-section of a single silica sphere.

(In the silica sol, TEOS/H_2O (w/w) = 3, HCl/H_2O = 100 mmol/L for a–c and HCl/H_2O = 10 mmol/L for d; in the aqueous phase, silica sol/monomer solution (w/w) = 2.5 for a–b and silica sol/monomer solution (w/w) = 3.0 for c–d.)

under different TEOS concentration in the silica sol are shown in Figure 6 and Figure 7. Under the relatively high TEOS concentration, the silica spheres have smooth external surface and compact internal structure. With the decrease of TEOS concentration, the structure of silica spheres becomes loose, and a large amount of texture pores emerge, since the size of the original organic-inorganic hybrid spheres had been fixed by the polyacrylamide framework. The solidification rate of droplets is reduced when TEOS concentration decreases, and the hybrid spheres tend to agglomerate under low TEOS concentration.

Figure 8 shows the SEM images of samples synthesized under lower HCl concentration in the silica sol. Compared with the corresponding samples (Figure 6d–f and Figure 7a–c), the samples synthesized by silica sol with lower acidity have more homogeneous structure, since the high pH condition facilitates the polymerization reaction of acrylamide.

All the aforementioned silica spheres have solid and homogeneous structure, for they were synthesized using the sedimentation medium containing 30 wt % TOA. Silica spheres with various morphology and structure can be obtained by changing the composition of sedimentation medium (Figure 9). Hollow silica spheres can be obtained when n-octanol or tri-n-butyl phosphate (TBP) was used together with liquid paraffin solution of TOA as sedimentation medium, because both octanol and TBP can extract large amount of substance, such as alcohol, even polymeric monomers and water from the droplets. However, these spheres have rough surface and weak mechanical stability. By lowering the acidity in the sol, the surface smoothness and mechanical stability of spheres can be much improved (comparing d with c).

Through the aforementioned results, the structure of silica spheres can be effectively adjusted by synthesis conditions: the textural structure of silica spheres can be adjusted by

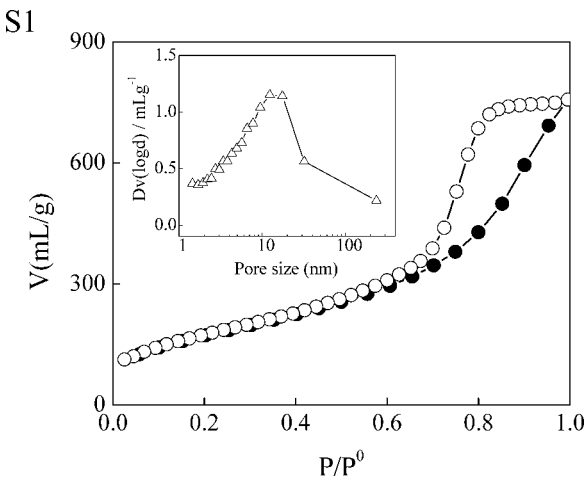

Figure 10. Nitrogen adsorption-desorption isotherm of S1, and its pore-size distribution calculated by the BJH method using the adsorption branches (inset).

Table 1. Synthetic Conditions and Physicochemical Properties of Representative Samples

	Silica Sol		Aqueous Phase	Physicochemical Properties*					
Sample	$TEOS/H_2O$ (w/w)	HCl/H_2O (mmol/L)	Silica sol/ monomer Solution (w/w)	S_{BET} (m^2/g)	V_{total} (mL/g)	D_A (nm)	D_{BJHA} (nm)	D_{BJHD} (nm)	V_{intru} (mL/g)
S1	3.0	100	2.5	627	1.16	7.4	12.4	9.0	0.82
S2	3.0	100	1.7	627	1.27	8.1	12.3	6.3	—
S3	3.0	10	2.5	590	1.12	7.6	12.1	9.9	—
S4	0.5	10	3.0	612	2.57	16.8	32.1	31.8	1.46
S5	1.2	100	3.0	555	2.36	17.0	32.0	17.7	1.58
S6	1.2	10	3.0	675	1.62	9.6	15.1	11.4	1.13

*S_{BET}: multipoint BET surface area; V_{total}: total pore volume; D_A: average pore diameter; D_{BJHA}: BJH method adsorption pore diameter; D_{BJHD}: BJH method desorption pore diameter; V_{intru}: mercury intrusion volume.

shifting the concentration of TEOS, HCl and polymeric monomer in the aqueous phase, and the homogeneity of silica spheres can be controlled by changing the composition of sedimentation medium.

Porous properties

Through the previous SEM observation, submicrometer-sized textural pores were found in parts of silica spheres. Detailed pore structure of silica spheres was determined by nitrogen adsorption-desorption and mercury intrusion measurements.

The nitrogen adsorption-desorption isotherm of the representative sample (S1) is plotted in Figure 10, which shows the distinct characteristic of mesoporous materials. The pore-size distribution calculated by the BJH method using adsorption branch shows a broad peak centered at about 15.1 nm (seen in the inset). The synthesis conditions of the representative samples and their physicochemical properties are listed in Table 1. All the silica spheres have high-surface area (>550 m^2/g), and large pore volume (>1.1 mL/g). The total pore volume, average pore diameter, and BJH pore diameter of silica spheres increase with the increase of monomer concentration, and the decrease of silica concentration in the aqueous phase. The total pore volume and the pore diameter of silica spheres decreases with the decrease of HCl concentration when the TEOS concentration is low. However, when the TEOS concentration is high, the influence of HCl concentration on the pore structure of silica spheres is slight. The effect of synthesis conditions on the structure of silica spheres is summarized in Table 2.

The effect of synthesis conditions on the pore structure of silica spheres can be characterized clearly by the mercury intrusion method. Intrusion volumes and pore-size distributions of silica spheres under various synthesis conditions are shown in Table 1 and Figure 11, from which large amount of macropores (>50 nm) of S4 and S5 can be seen evidently.

Discussion of mechanism

The mechanism of the synthesis method is proposed based on the previous results, and the mechanism of "pH-induced rapid colloid aggregation" method discussed in our previous research.[33,34] The scheme of the formation process of silica spheres is shown in Figure 12.

In the prehydrolysis process, mesostructured primary silica particles are formed through counterion-mediated $S^+X^-I^+$ assembly route using F127 and PEG as templates, and silica sol are accordingly obtained. In the sedimentation process, polymeric monomers in the droplets polymerize rapidly in the hot alkali sedimentation medium. Silica sol is kept in the hybrid spheres and slowly solidifies. Mesostructured counterion-mediated assemblies in the silica sol may be damaged by alkali in the sedimentation medium. Accordingly, the mesopores in resultant silica spheres become larger.

Polymerization speed of acrylamide monomer is an important factor in this synthesis process. If polymerization rate is accelerated, the droplets can be solidified more rapidly and the mesostructured counterion-mediated assemblies can be well protected. Polymerization speed can be effectively controlled by varying the concentration of polymeric monomers and acid in the aqueous phase to obtain silica spheres with different pore structure.

The silica spheres obtain macropores due to the removal of the polymer by calcination. The macropores structure mainly depends on the concentration of silica source and polymeric monomers in the aqueous phase. Silica spheres with large pore volume can be synthesized with high-polymeric monomer concentration and low-silica concentration.

Protein adsorption

Silica spheres synthesized in this work have the advantages of both high surface areas and large pore volumes, which are quite suitable for adsorption of large biomolecules.

Table 2. The Effect of Synthesis Conditions on the Structure of Silica Spheres*

Synthesis Condition		Compactness of Structure	Total Pore Volume	Average Pore Size
TEOS concentration	↑	↑	↓	↓
Monomer concentration	↑	↓	↑	↑
pH in the silica sol (when TEOS concentration is high)	↑	–	–	–
pH in the silica sol (when TEOS concentration is low)	↑	↑	↓	↓

*↑: the trend of increase; ↓: the trend of decrease; –: no change.

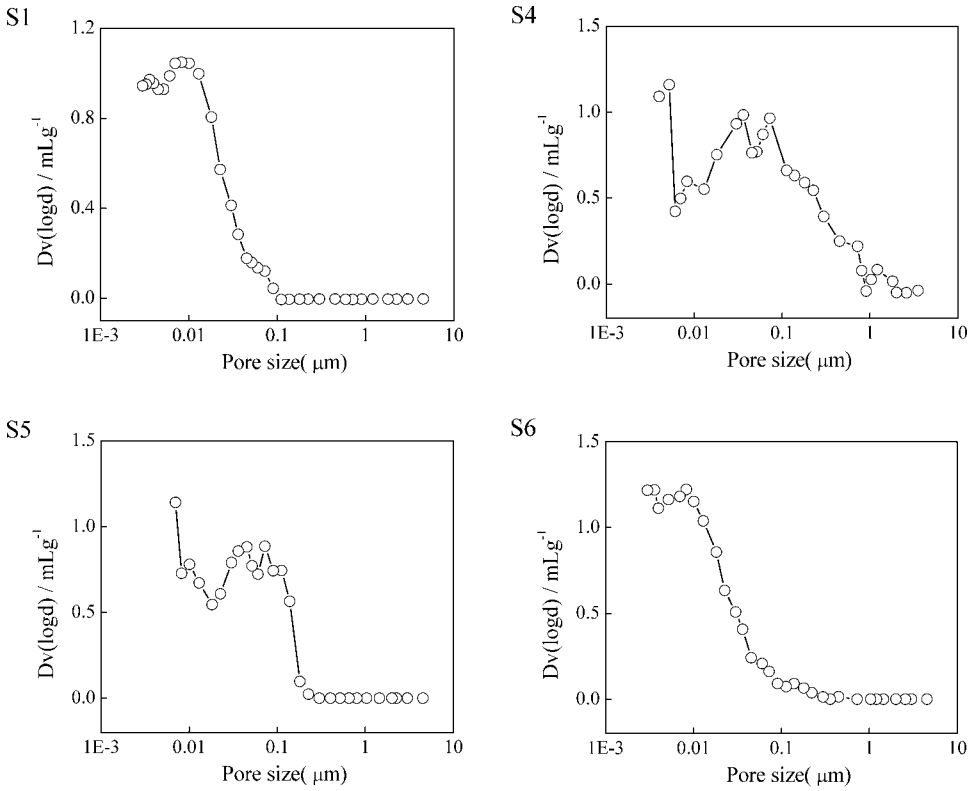

Figure 11. Pore-size distributions of representative samples between 3.0 nm and 5.0 μm determined by mercury intrusion method. S1, S4, S5 and S6 are denoted in Table 1.

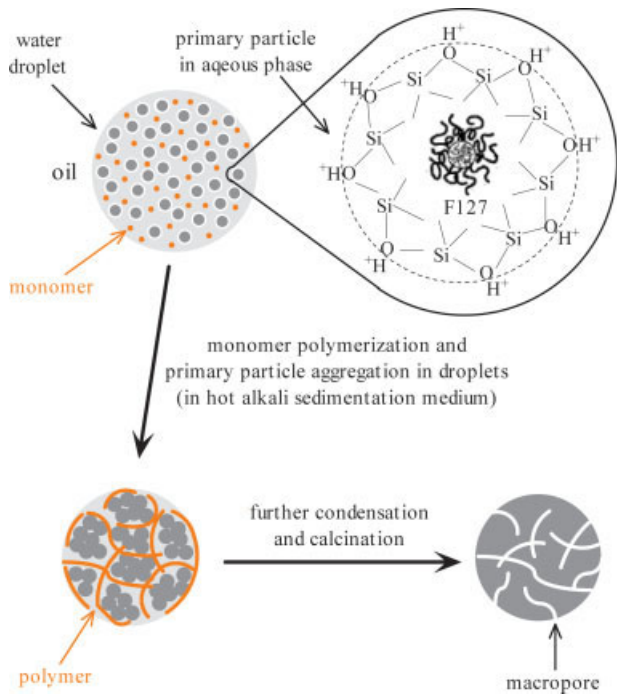

Figure 12. Probable scheme of the formation process of silica spheres.

[Color figure can be viewed in the online issue, which is available at www.interscience.wiley.com.]

To investigate the adsorption capacity of large biomolecules on the silica spheres, BSA was used as a model protein in the adsorption experiment. BSA is a large protein with the molecular weight of 69 kDa, and the dimensions of 4 nm × 4 nm × 14 nm.[53] Sample S4, S5 and S6 are tested to determine the effect of pore structure on the protein adsorption capacity.

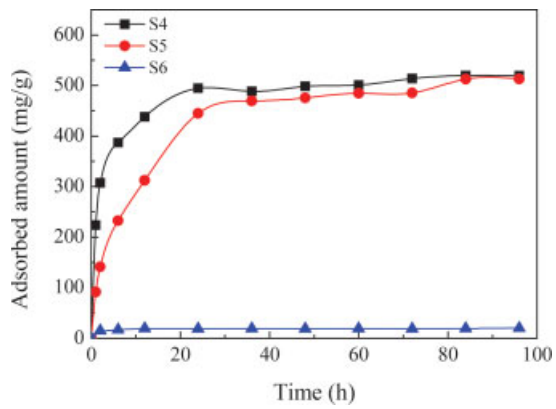

Figure 13. BSA adsorption kinetics on representative samples at pH 5.0 with 50 mM acetate buffer for 96 h with initial BSA concentration of 10 mg/mL.

[Color figure can be viewed in the online issue, which is available at www.interscience.wiley.com.]

Table 3. Amount of BSA Adsorbed onto Representative Samples and Adsorbed BSA Occupied Volume

Sample	BSA Adsorbed (mg/g)	Volume Occupied V_{BSA} (mL/g)	V_{total} (mL/g)	V_{BSA} / V_{total} %
S4	520	0.53	2.57	21
S5	513	0.53	2.36	22
S6	20	0.02	1.62	1

Adsorption kinetics of BSA on the three materials at pH 5.0 are shown in Figure 13. This pH value is close to the isoelectric point of BSA (pI = 4.9), and the repulsive electrostatic interaction between protein and adsorbent is minimum under the condition. High-adsorption capacity, as high as 520 mg/g and 513 mg/g, respectively, of S4 and S5 for BSA has been obtained. The equilibrium capacity of S6 is only 20 mg/g, which is much lower than that of S4 and S5. Theoretical volume occupied by BSA in the silica spheres has been calculated assuming the BSA molecule to be an ellipsoid with the size of 4 nm × 4 nm × 14 nm, and the results are listed in Table 3. BSA molecules occupy about 20% of total volume in S4 and S5, but only 1% of total volume in S6.

To investigate whether BSA molecules enter the pores of spheres or just adsorb on the external surface of silica spheres, nitrogen adsorption-desorption isotherms of samples before and after BSA adsorption are shown in Figure 14, and the physicochemical properties of samples before and after BSA adsorption are compared in Table 4. The remarkable decrease of total pore volume and surface area of S4 and S5 after BSA adsorption evidently demonstrate that BSA molecules have occupied part of pore volume. The amount of reduced volume is much larger than the theoretical volume occupied by BSA in Table 3, because some BSA molecules may block the entrance of the micropores and small mesopores in silica spheres. Since the external surface area of the spheres is very low (<0.05 m^2/g), almost all BSA molecules must be adsorbed in the pores of silica spheres.

Therefore, pore size of spheres has crucial influence on the adsorption process. High-protein adsorption capacity is determined by two factors: (1) plenty of texture pores on the external surface of silica spheres to make full use of the internal structure, and (2) large entrances of mesopores to ensure large amount of mesopores available for protein adsorption. The SEM images of external surface of S4, S5 and S6 are shown in Figure 15, and the size of entrance of mesopores can be determined by D_{BJHD} in Table 1. There are high content of texture pores on the external surface of S4 and S5, and the entrances of their mesopores are also large enough for BSA adsorption, so BSA molecules can enter most pores of these spheres. However, S6 has few texture pores on the external surface, so BSA molecules are excluded from the surface of silica spheres. A large part of internal structure is not available for protein adsorption. Hence, the adsorption amount of S4 and S5 is much larger than that of S6. The adsorption rate for S5 is slower than S4

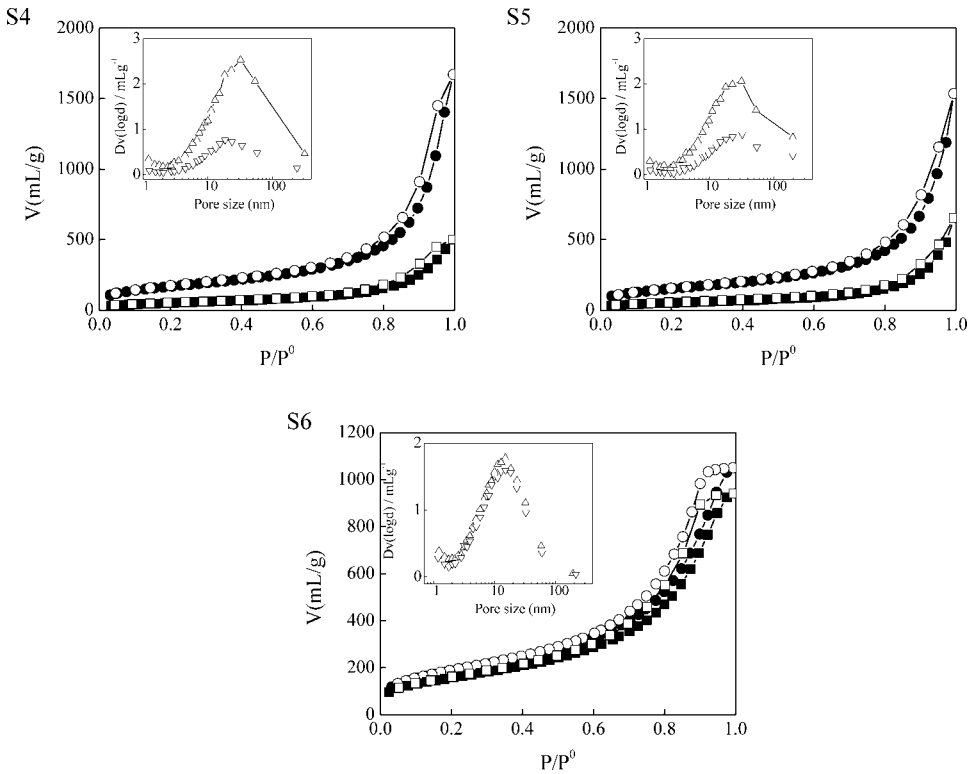

Figure 14. Nitrogen adsorption-desorption isotherms of representative samples before and after BSA adsorption and their pore-size distributions calculated by the BJH method using the adsorption branches (insets).

S4, S5 and S6 are denoted in Table 2. (●, ■) the point on the adsorption isotherm, (○, □) the point on the desorption isotherm; (●, ○, △) before BSA adsorption, (■, □, ▽) after BSA adsorption.

Table 4. Physicochemical Properties of Representative Samples Before and After BSA Adsorption*

	Before Adsorption					After Adsorption				
Sample	S_{BET} (m^2/g)	V_{total} (mL/g)	D_A (nm)	D_{BJHA} (nm)	D_{BJHD} (nm)	S_{BET} (m^2/g)	V_{total} (mL/g)	D_A (nm)	D_{BJHA} (nm)	D_{BJHD} (nm)
S4	612	2.57	16.8	32.1	31.8	190	0.77	16.2	18.5	17.4
S5	555	2.36	17.0	32.0	17.7	193	1.01	20.9	32.8	17.3
S6	675	1.62	9.6	15.1	11.4	572	1.45	10.1	15.1	12.4

*S_{BET}: multipoint BET surface area; V_{total}: total pore volume; D_A: average pore diameter; D_{BJHA}: BJH method adsorption pore diameter; D_{BJHD}: BJH method desorption pore diameter.

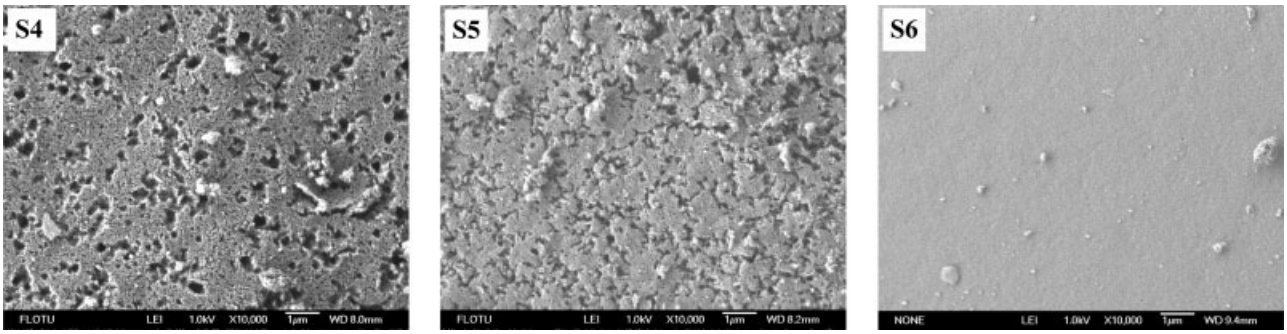

Figure 15. SEM images of external surface of the representative samples. S4, S5 and S6 are denoted in Table 1.

in the first day although their equilibrium amounts are almost the same because S4 has the larger BJH pore diameter. High-surface area leads to the high-protein adsorption capacity of S4 and S5, but it is not the key issue to determine the adsorption capacity because there is not much difference among the surface area of these samples. Pore volume has little influence here since only a small part of total pore volume has been used in the protein adsorption.

Conclusion

We developed a new two-stage method to synthesize mesoporous silica spheres. A silica sol was made by prehydrolysis of TEOS in an aqueous acidic solution using a triblock copolymer as the template. Then, drops of the silica sol were injected by a microfluidic device into a heated oil bath, where the droplets solidified during sedimentation. Micrometer-sized mesoporous silica spheres with uniform diameters and adjustable pore structure were successfully synthesized with the assistance of the microfluidic device and the acrylamide polymerization reaction. Synthesis conditions have great influence on the morphology and the pore structure of spheres. Silica spheres with different morphology were obtained by changing the composition of sedimentation medium, such as adding new coextractants. Pore structure can be adjusted effectively by controlling the composition of aqueous phase, such as the concentration of silica source, acid or polymeric monomer. With the decrease of TEOS concentration or the increase of acid or monomer concentration, the pore diameter of spheres is enlarged. The prepared silica spheres have high-surface area, large pore volume, robust framework, homogeneous structure and a large amount of macropores. High-protein adsorption capacity of spheres has been achieved in the adsorption experiments of BSA, and a large amount of protein molecules are demonstrated to be adsorbed in the pores of spheres. Pore structure of spheres is a crucial factor to determine the protein adsorption capacity.

Acknowledgments

We acknowledge the financial support from the National Natural Science Foundation of China (20676066 and 20525622) and National Basic Research Program of China (2007CB714302) on this work gratefully.

Literature Cited

1. Kresge CT, Leonowicz ME, Roth WJ, Vartuli JC, Beck JS. Ordered mesoporous molecular sieves synthesized by a liquid-crystal template mechanism. *Nature*. 1992;359:710–712.
2. Beck JS, Vartuli JC, Roth WJ, Leonowicz ME, Kresge CT, Schmitt KD, Chu CTW, Olson DH, Sheppard EWJ. A new family of mesoporous molecular sieves prepared with liquid crystal templates. *J Am Chem Soc*. 1992;114:10834–10843.
3. Davis ME. Ordered porous materials for emerging applications. *Nature*. 2002;417:813–821.
4. Stein A. Advances in microporous and mesoporous solids - Highlights of recent progress. *Adv Mater*. 2003;15:763–775.
5. Hartmann M. Ordered mesoporous materials for bioadsorption and biocatalysis. *Chem Mater*. 2005;17:4577–4593.
6. Tortajada M, Ramon N, Beltran D, Amoros P. Hierarchical bimodal porous silicas and organosilicas for enzyme immobilization. *J Mater Chem*. 2005;15:3859–3868.
7. Deere J, Magner E, Wall JG, Hodnett BK. Adsorption and activity of cytochrome c on mesoporous silicates. *Chem Commum*. 2001: 465–466.
8. Deere J, Magner E, Wall JG, Hodnett BK. Adsorption and activity of proteins onto mesoporous silica. *Catal Lett*. 2003;85:19–23.
9. Vinu A, Murugesan V, Tangermann O, Hartmann M. Adsorption of cytochrome c on mesoporous molecular sieves: Influence of pH,

pore diameter, and aluminum incorporation. *Chem Mater*. 2004; 16:3056–3065.
10. Washmon-Kriel L, Jimenez VL, Balkus KJ. Cytochrome c immobilization into mesoporous molecular sieves. *J Mol Catal B*. 2000;10: 453–469.
11. Qiao SZ, Yu CZ, Xing W, Hu QH, Djojoputro H, Lu GQ. Synthesis and bio-adsorptive properties of large-pore periodic mesoporous organosilica rods. *Chem Mater*. 2005;17:6172–6176.
12. Vinu A, Murugesan V, Hartmann M. Adsorption of lysozyme over mesoporous molecular sieves MCM-41 and SBA-15: Influence of pH and aluminum incorporation. *J Phys Chem B*. 2004;108:7323–7330.
13. Fan J, Lei J, Wang L, Yu C, Tu B, Zhao D. Rapid and high-capacity immobilization of enzymes based on mesoporous silicas with controlled morphologies. *Chem Commum*. 2003:2140–2141.
14. Kisler JM, Dahler A, Stevens GW, O'Connor AJ. Separation of biological molecules using mesoporous molecular sieves. *Micropor Mesopor Mater*. 2001;44:769–774.
15. Goradia D, Cooney J, Hodnett BK, Magner E. The adsorption characteristics, activity and stability of trypsin onto mesoporous silicates. *J Mol Catal B*. 2005;32:231–239.
16. Gomez JM, Deere J, Goradia D, Cooney J, Magner E, Hodnett BK. Transesterification catalyzed by trypsin supported on MCM-41. *Catal Lett*. 2003;88:183–186.
17. Katiyar A, Ji L, Smirniotis P, Pinto NG. Protein adsorption on the mesoporous molecular sieve silicate SBA-15: effects of pH and pore size. *J Chromatogr A*. 2005;1069:119–126.
18. Chong ASM, Zhao XS. Design of large-pore mesoporous materials for immobilization of penicillin G acylase biocatalyst. *Catalysis Today*. 2004;93–95:293–299.
19. Aburto J, Ayala M, Bustos-Jaimes I, Montiel C, Terres E, Domınguez JM, Torres E. Stability and catalytic properties of chloroperoxidase immobilized on SBA-16 mesoporous materials. *Micropor Mesopor Mater*. 2005;83:193–200.
20. Pandya PH, Jasra RV, Newalkar BL, Bhatt PN. Studies on the activity and stability of immobilized alpha-amylase in ordered mesoporous silicas. *Micropor Mesopor Mater*. 2005;77:67–77.
21. Singh PS, Kosuge K. The synthesis of mesoporous silica spheres by octylamine templating. *Chem Lett*. 1998:101–102.
22. Kosuge K, Singh PS. Rapid synthesis of Al-containing mesoporous silica hard spheres of 30–50 μm diameter. *Chem Mater*. 2001;13: 2476–2482.
23. Kosuge K, Singh PS. Mesoporous silica spheres via l-alkylamine templating route. *Micropor Mesopor Mater*. 2001;44:139–145.
24. Kosuge K, Murakami T, Kikukawa N, Takemori M. Direct synthesis of porous pure and thiol-functional silica spheres through the $S^+X^-I^+$ assembly pathway. *Chem Mater*. 2003;15:3184–3189.
25. Schacht S, Huo Q, Voigt-Martin IG, Stucky GD, Schüth F. Oil-water interface templating of mesoporous macroscale structures. *Science*. 1996;273:768–771.
26. Izutsu H, Mizukami F, Nair PK, Kiyozumi Y, Maedab K. Preparation and characterization of porous silica spheres by the sol-gel method in the presence of tartaric acid. *J Mater Chem*. 1997;7:767–771.
27. Fowler CE, Khushalani D, Mann S. Interfacial synthesis of hollow microspheres of mesostructured silica. *Chem Commun*. 2001:2028–2029.
28. Li W, Sha X, Dong W, Wang Z. Synthesis of stable hollow silica microspheres with mesoporous shell in nonionic W/O emulsion. *Chem Commun*. 2002:2434–2435.
29. Qi L, Ma J, Cheng H, Zhao Z. Micrometer-sized mesoporous silica spheres grown under static conditions. *Chem Mater*. 1998:10:1623–1626.
30. Lin HP, Cheng YR, Mou CY. Hierarchical order in hollow spheres of mesoporous silicates. *Chem Mater*. 1998:10:3772–3776.
31. Sun QY, Kooyman PJ, Grossmann JG, Bomans PHH, Frederik PM, Magusin PCMM, Beelen TPM, van Santen RA, Sommerdijk NAJM. The formation of well-derined hollow silica spheres with multilamellar shell structure. *Adv Mater*. 2003:15:1097.
32. Sun QY, Magusin PCMM, Mezari B, Panine P, van Santen RA, Sommerdijk NAJM. The formation of gigantic hollow silica spheres from an EO_{76}-$PO_{29}EO_{76}$/butanol/ethanol/H_2O quaternary system. *J Mater Chem*. 2005:15:256–259.
33. Yang LM, Wang YJ, Luo GS, Dai YY. A new 'pH-induced rapid colloid aggregation' method to prepare micrometer-sized spheres of mesostructured silica in water-in-oil emulsion. *Micropor Mesopor Mater*. 2006;94:269–276.
34. Yang LM, Wang YJ, Sun YW, Luo GS, Dai YY. Synthesis of micrometer-sized hard silica spheres with uniform mesopore size and textural pores. *J Colloid Interf Sci*. 2006;299:823–830.
35. Lind A, von Hohenesche CD, Smått JH, Lindén M, Unger K. Spherical silica agglomerates possessing hierarchical porosity prepared by spray drying of MCM-41 and MCM-48 nanospheres. *Micropor Mesopor Mater*. 2003;66:219–227.
36. Boissière C, van der Lee A, El Mansouri A, Larbot A, Prouzet E. A double step synthesis of mesoporous micrometric spherical MSU-X silica particles. *Chem Commun*. 1999:2047–2048.
37. Boissière C, Larbot A, van der Lee A, Kooyman PJ, Prouzet E. A new synthesis of mesoporous MSU-X silica controlled by a two-step pathway. *Chem Mater*. 2000;12:2902–2913.
38. Boissière C, Larbot A, Bourgaux C, Prouzet E, Bunton CA. A study of the assembly mechanism of the mesoporous MSU-X silica two-step synthesis. *Chem Mater*. 2001;13:3580–3586.
39. Martin T, Galarneau A, Di Renzo F, Fajula F, Plee D. Morphological control of MCM-41 by pseudomorphic synthesis. *Angew Chem-Int Edit*. 2002;41:2590–2592.
40. Lefevre B, Galarneau A, Iapichella J, Petitto C, Di Renzo F, Fajula F, Bayram-Hahn Z, Skudas R, Unger K. Synthesis of large-pore mesostructured micelle-templated silicas as discrete spheres. *Chem Mater*. 2005;17:601–607.
41. Petitto C, Galarneau A, Driole MF, Chiche B, Alonso B, Di Renzo F, Fajula F. Synthesis of discrete micrometer-sized spherical particles of MCM-48. *Chem Mater*. 2005;17:2120–2130.
42. Lewis PC, Graham RR, Nie ZH, Xu SQ, Seo M, Kumacheva E. Continuous synthesis of copolymer particles in microfluidic reactors. *Macromolecules*. 2005;38:4536–4538.
43. Nisisako T, Torii T, Higuchi T. Novel microreactors for functional polymer beads. *Chem Eng J*. 2004;101:23–29.
44. Nie ZH, Xu SQ, Seo M, Lewis PC, Kumacheva E. Polymer particles with various shapes and morphologies produced in continuous microfluidic reactors. *J Am Chem Soc*. 2005;127:8058–8063.
45. Jeong WJ, Kim JY, Choo J, Lee EK, Han CS, Beebe DJ, Seong GH, Lee SH. Continuous fabrication of biocatalyst immobilized microparticles using photopolymerization and immiscible liquids in microfluidic systems. *Langmuir*. 2005;21:3738–3741.
46. Dendukuri D, Tsoi K, Hatton TA, Doyle PS. Controlled synthesis of nonspherical microparticles using microfluidics. *Langmuir*. 2005;21: 2113–2116.
47. Xu SQ, Nie ZH, Seo M, Lewis PC, Kumacheva E, Stone HA, Garstecki P, Weibel DB, Gitlin I, Whitesides GM. Generation of monodisperse particles by using microfluidics: Control over size, shape, and composition. *Angew Chem Int Ed*. 2005;44:724–728.
48. Seo M, Nie ZH, Xu SQ, Mok M, Lewis PC, Graham R, Kumacheva E. Continuous microfluidic reactors for polymer particles. *Langmuir*. 2005;21:11614–11622.
49. Quevedo E, Steinbacher J, McQuade DT. Interfacial polymerization within a simplified microfluidic device: Capturing capsules. *J Am Chem Soc*. 2005;127:10498–10499.
50. Nisisako T, Torii T, Takahashi T, Takizawa Y. Synthesis of monodisperse bicolored janus particles with electrical anisotropy using a microfluidic co-flow system. *Adv Mater*. 2006;18:1152.
51. Utada AS, Lorenceau E, Link DR, Kaplan PD, Weitz DA. Monodisperse double emulsions generated from a microcapillary device. *Science*. 2005;308:537–541.
52. Zhang HF, Hardy GC, Rosseinsky MJ, Cooper AI. Uniform emulsion-templated silica beads with high pore volume and hierarchical porosity. *Adv Mater*. 2003;15:78.
53. Tarasevich YI. Interaction of globular albumins with the silica surface. *Theor Exp Chem*. 2001;37:98–102.

Manuscript received July 30, 2007, and revision received Sept. 29, 2007.